ORIGINAL ARTICLE

Influence of post-pyrolysis treatment on physicochemical properties and acid medium stability of magnetic carbon nanocomposites

A. A. Burbano[1] · G. A. Muñoz Medina[2] · F. H. Sánchez[2] · V. L. Lassalle[1] · M. F. Horst[1] · G. Gascó[3] · A. Méndez[4]

Abstract

This study presents the preparation of magnetic carbon nanocomposites (MCNCs) through a two-step procedure: (i) in situ co-precipitation of magnetite (Fe_3O_4) nanoparticles into four different carbonaceous matrixes and (ii) post-pyrolysis treatment to coat the magnetic core. Four post-pyrolysis MCNCs were obtained: MACP (post-pyrolyzed magnetic activated carbon), MCCP (post-pyrolyzed magnetic charcoal), $MHCP_{OR}$ (post-pyrolyzed magnetic hydrochar from orange residue), and $MBCP_{SFH}$ (post-pyrolyzed magnetic biochar from sunflower husk). These four samples were compared with the starting MCNCs prepared without post-pyrolysis treatment: MAC, MCC, MHC_{OR}, and MBC_{SFH}, respectively. After post-pyrolysis treatment, a thin carbon layer surrounding some of the magnetite nanoparticles was identified by transmission electron microscopy. Post-pyrolysis modified the porous structure and chemical composition of MCNCs. Furthermore, a leaching test with acid sulfuric solution at 90 °C was carried out. The results suggested that the $MHCP_{OR}$ and $MBCP_{SFH}$ were more stable in an acidic medium than MACP and MCCP, indicating that the coat generated during post-pyrolysis of hydrochar and biochar could partially protect the magnetic core by reducing Fe leaching into the aqueous solution. Biochar and the hydrochar-based MCNCs before and after post-pyrolysis treatment exhibit superparamagnetic properties; however, their saturation magnetization (M_s) decreased considerably. These results open the potential application fields of MCNCs obtained by post-pyrolysis of biochar and hydrochar-based materials in acidic mediums.

Keywords Pyrolysis · Hydrothermal carbonization · Magnetic nanocomposite · Biochar · Hydrochar · Stability

1 Introduction

Nanotechnology and nanoscience have evoked great interest in the scientific community since materials at nanodimensions (1–100 nm) enhance their physicochemical properties that differ from bulk materials. Different nanomaterials have been synthesized, particularly the iron oxide nanoparticles (IONPs) which are applied in different fields such as electronics, biomedicine, and environmental remediation [1, 2]. Magnetite (Fe_3O_4) has gained special attention among iron oxide nanoparticles due to its high surface area-to-volume ratio, chemical stability, superparamagnetic behavior, and biocompatibility [3]. Nevertheless, they exhibit drawbacks, such as aggregation trends, resulting from their high surface area and magnetic dipole interactions between particles. Moreover, when exposed to air, magnetite can be easily oxidized to maghemite (γ-Fe_2O_3). Furthermore, leasing these metal nanoparticles could cause secondary pollution, limiting their potential uses [4]. Thus, exploring suitable porous materials as stabilizers and carriers is necessary to support IONPs. Magnetic porous materials can be further employed as adsorbents or catalysts in different chemical processes [5, 6].

Activated carbons are unique carrier materials due to their excellent ability to support nanoparticles, stability, high surface area, and porous structure [7, 8]. However, commercial activated

✉ A. Méndez
anamaria.mendez@upm.es

1 INQUISUR, Departamento de Química, Universidad Nacional del Sur (UNS)-CONICET, Av. Alem 1253, 8000 Bahía Blanca, Argentina

2 Departamento de Física, Instituto de Física La Plata IFLP-CONICET, Universidad Nacional de La Plata, Buenos Aires, Argentina

3 Departamento de Producción Agraria, Universidad Politécnica de Madrid, Ciudad Universitaria, 28040 Madrid, Spain

4 Departamento Ingeniería Geológica y Minera. E.T.S.I. Minas y Energía, Universidad Politécnica de Madrid, Calle Ríos Rosas, 21-Madrid, 28003 Madrid, Spain

carbons are expensive due to the feedstock manufacturing characteristics and activation processes. These disadvantages have caused the exhaustive finding of economically low-cost alternatives like carbonaceous materials (biochars and hydrochars) prepared by thermochemical treatments of biomass wastes [9, 10]. These materials can be applied in many fields, including soil amendment and adsorption of pollutants in water, soil, and atmosphere [11, 12]. However, it would be interesting to extend its use to adsorption processes of pollutants in acid mine water and as catalysts in hydrometallurgical processes [13, 14].

It has been established that a proper coating of IONPs by carbonaceous structures can improve their stability and protect the magnetic core of IONPs from oxidation and disaggregation [15, 16]. Several studies have pointed out the importance of employing a carbon layer since it is (i) practical, (ii) biocompatible, and (iii) would lead to reducing the damage of the magnetic core when exposed to aggressive conditions [17–19]. To achieve a proper coating of the magnetic core, a wide range of treatments are available, including chemical vapor deposition, solution plasma processing, hydrothermal methods, spray pyrolysis, and solid-phase synthesis [20–22]. It has been demonstrated that IONP encapsulation employing different coatings based on citric acid, lactonic acid, polyvinylpyrrolidone, or polyethylene glycol enhances the chemical, thermal, and colloidal stabilities [23, 24]. The treatments mentioned above are well known and efficient. Nonetheless, they are time- and cost-consuming. Therefore, this study aims to use an economical, operationally easy, and efficient treatment such as slow pyrolysis as a post-thermal treatment of magnetic carbonaceous materials to coat the magnetic core with carbon [25]. In the post-thermal treatment, volatile compounds are generated, contributing to the coat formation. It is hypothesized that released volatiles are also in charge of coating the magnetic nanoparticles reducing the damage of IONPs in an acidic medium. For this reason, a leaching experiment was designed to control iron dissolution in an acidic medium. Magnetic carbon nanocomposites before and after post-pyrolysis treatment underwent an exhaustive characterization, employing spectroscopic and microscopic techniques. We hypothesized that post-pyrolysis treatment of magnetic carbon nanocomposites can increase their stability in acidic medium and can open the potential application fields of magnetic carbon nanocomposites in acidic mediums such as adsorbents in acid mine water and hydrometallurgical processes and the preparation of advanced materials from biomass wastes.

2 Materials and methods

2.1 Materials

Sulfuric acid (H_2SO_4 96%) and iron (II) sulfate heptahydrate ($FeSO_4 \cdot H_2O$) was supplied from Labkem (Barcelona, Spain). Iron (III) chloride 6-hydrate ($FeCl_3.6H_2O$) was purchased from PanReac AppliChem (Barcelona, Spain), and sodium hydroxide (NaOH) was supplied by Merck (Darmstadt, Germany). Commercial activated carbon was purchased from PanReac (Barcelona, Spain), and commercial charcoal was obtained from Ibecosl (Spain). The orange residue (OR) was supplied by one company of orange juice production located in southwest Spain, and sunflower husk (SFH) was supplied by a company of sunflower oil production located in Argentina.

2.2 Preparation of biochar and hydrochar

The feedstocks (orange residue and sunflowers husk) were washed, dried at 40 °C, and sieved until a homogeneous grain size (< 2 mm). The biochar (BC_{sfh}) was prepared by pyrolysis of SFH. For this purpose, a certain amount of SFH was placed into closed ceramic crucibles that were further introduced into a nickel container and covered with coke particles to accomplish an inert atmosphere. Samples were placed in a muffle and heated until 700 °C. The final temperature was maintained for 2.5 h.

Hydrochar from the orange residue (HC_{OR}) was prepared as follows: 1.0 L of wet orange residue solution with 30% solid content was introduced in a Teflon recipient inside a Hastelloy autoclave supplied by Demede S.L. The autoclave has two thermocouples, one is inserted into the Teflon recipient in contact with the sample, and another is in contact with the outer part of the Hastelloy wall. The temperature difference between the two thermocouples is around 20 °C. Samples were heated at 240 °C, and the final temperature was maintained for 6 h. After cooling down to room temperature, the aqueous solutions were filtered, and the hydrochar was dried at 90 °C for 24 h.

2.3 Preparation of magnetic carbon nanocomposites

The four magnetic carbonaceous materials, magnetic biochar obtained from sunflower husk (MBC_{SFH}), magnetic hydrochar obtained from the orange residue (MHC_{OR}), magnetic activated carbon (MAC), and magnetic charcoal (MCC), were performed by in situ co-precipitation of magnetite nanoparticles into corresponding carbonaceous solid (BC_{SFH}, HC_{OR}, CAC, and CC, respectively). For this purpose, $FeCl_3.6H_2O$ and $FeSO_4.7H_2O$ in a ratio of 2:1 were mixed and stirred with the carbonaceous solid until homogeneous dispersion. Further on, NaOH 5 M was added dropwise to obtain the magnetic carbonaceous materials.

2.4 Post-pyrolysis treatment of magnetic carbon nanocomposites

Four post-pyrolyzed magnetic carbonaceous materials, MBCP$_{SFH}$, MHCP$_{OR}$, MACP, and MCCP, were prepared by post-pyrolysis of MBC$_{SFH}$, MHC$_{OR}$, MAC, and MCC, respectively. The experimental procedure was adapted from Luis M. Martínez-Prieto [26]. First, a known amount of each magnetic carbonaceous material (MBC$_{SFH}$, MHC$_{OR}$, MAC, and MCC) was weighed and pyrolyzed in an inert atmosphere at 600 °C using a heating rate of 15 °C s^{-1}. The final temperature was maintained for 2 h, and the final product was collected, sieved, and saved in flasks. Figure 1 shows the two main steps involved in preparing both kinds of magnetic carbonaceous materials.

2.5 Characterization of post-pyrolyzed magnetic carbon nanocomposites

Characterization of magnetic carbon nanocomposites without (MBC$_{SFH}$, MHC$_{OR}$, MAC, and MCC) and with post-pyrolysis treatment (MBCP$_{SFH}$, MHCP$_{OR}$, MACP, and MCCP) was performed as follows: carbon, hydrogen, nitrogen, and sulfur contents were determined by dry combustion using a LECO CHNS 932 Analyzer (SCAI-Malaga University, Spain). Oxygen was obtained by difference as 100%-(%C + %H + %N + %S + %Ash). In addition, atomic ratios (H/C) and (O/C) were calculated. pH, redox potential (Eh), and electrical conductivity (σ) of carbonaceous magnetic carbons were determined on aqueous solutions at a concentration of 4 g L^{-1} of a carbonaceous sample in distilled water solution using a Crison micro pH 2000, a pH 60 DHS, and EQUIPO EC, respectively. Besides, ash content was calculated by heating the samples at 800 °C for 24 h in a muffle. The relative ash content was then calculated as follows:

$$Ash(\%) = \frac{(weight\ of\ samples\ at\ 800^{\circ}C)}{(initial\ weight\ of\ sample)} * 100\% \quad (1)$$

The presence of functional groups of the materials was studied by Fourier transform infrared (FTIR) spectroscopy using a spectrophotometer Vertex 70 (Bruker). For the acquisition of spectra, a standard spectral resolution of 4 cm^{-1} was used in the spectral range of 4000–400 cm^{-1} and 64 accumulations per sample. The crystal structure was determined by an X-ray diffractometer (XRD; SmartLab3KW, Rigaku D, Japan). The BET surface area and pore size were used to determine the porous structure of the materials through N$_2$ adsorption–desorption experiments using a Porosimetry System ASAP2460, Atlanta, USA (SCAI Universidad de Málaga). Transmission electron microscopy (TEM Jeol 100 CX II) was employed to study the materials topographically and morphologically. Zeta potential as a pH function was carried out using a zeta potential analyzer (Nano-ZS90X, Malvern, UK). Magnetization curves, expressing specific magnetization (M) as a function of applied magnetic field (H) at room temperature, were obtained using a vibrating sample magnetometer (VSM) LakeShore 7404 operated with maximum applied fields μ0Hmax = 1.8 T.

2.6 Stability studies of magnetic carbon nanocomposites in acidic medium

Stability tests in an acidic medium of magnetic carbonaceous materials were carried out. First, 5 g of each sample was put in contact with 100 mL of H$_2$SO$_4$ 0.5 M, and the temperature was set at 90 °C according to temperatures used in potential applications of magnetic carbon nanocomposites as catalysts [13, 14]. Furthermore, aliquots were taken every 2, 4, 6, 24, and 48 h to quantify the concentration of Fe (mg L^{-1}) in the solution using an Analyst 400 PerkinElmer (AAS) spectrometer.
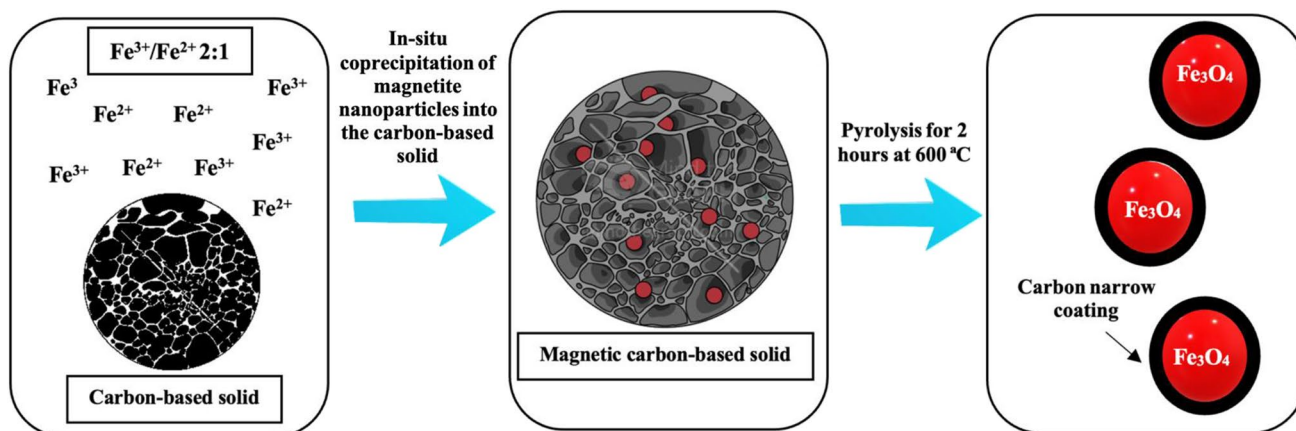

Fig. 1 Two main steps to preparing the post-pyrolyzed magnetic carbon nanocomposites

3 Results and discussion

3.1 Characterization of magnetic carbon nanocomposites

3.1.1 Morphology

TEM micrographs of magnetic carbon nanocomposites are displayed in Fig. 2. All the micrographs expose nanoparticle agglomeration. The nature of magnetic nanoparticles could explain this agglomeration as they possess high surface energy and exhibit dipole–dipole attraction [27–29]. For both reasons, they adhere and create significant clusters that could affect the further application or not. In this specific case, the formation of clusters was not the main issue. On the other side, in Fig. 2 (a1), goethite (α-FeOOH) intermediates appear as anisotropic crystals (needle-shaped) and magnetite as isotropic and topotactic structures [30]. Most micrographs exposed different particle sizes ranging from 5 to 50 nm. As seen in micrographs a2, b2, c2, and d2, magnetic carbon nanocomposites were post-pyrolyzed, goethite crystals almost disappeared, suggesting that under 600 °C, goethite undergoes chemical, structural, and crystalline transformations [31]. Some studies have shown that under temperature, goethite can be transformed into hematite (α-Fe$_2$O$_3$) [32, 33], indicating that some of the goethite phases are converted into hematite phases.

On the other hand, the post-pyrolyzed magnetic carbon nanocomposites seem different from the non-pyrolyzed materials. "Core–shell" structures can be seen in micrographs a2, b2, c2, and d2 (Fig. 2), where a thin carbon coating encapsulates the magnetite nanoparticles. It is most evident in Fig. 2 (d2). However, the carbon coating might not be homogeneous over the whole nanoparticle. This point is consistent with previous studies [34], where researchers prepared magnetic nanoparticles encapsulated in carbon that, through a slow pyrolysis treatment, magnetite nanoparticles were covered with a thin carbon layer that ranges from 2 to 5 nm. Post-pyrolysis treatment of carbonaceous matrix releases volatiles that are the ones that create the carbon coating surrounding the magnetic core. However, the carbon layer was not continuous, with cracks and gaps appearing [31].

3.1.2 Physicochemical characteristics of magnetic carbon nanocomposites

Table 1 shows the elemental analysis of magnetic carbon nanocomposites. The results indicate that the carbon and hydrogen content decreased after post-pyrolysis treatment. However, the oxygen content of MAC increases with post-pyrolysis from 2.37 to 9.28, whereas for MCC, MHC$_{OR}$, and MBC$_{SFH}$, the oxygen content decreases during post-pyrolysis treatment. Carbonaceous structures' changes in carbon, hydrogen, nitrogen, sulfur, and oxygen percentage are indicators of chemical transformations (condensation, volatilization, and decarboxylation). Post-pyrolysis treatment also produces ash enrichment, especially for MHC$_{OR}$, due to lower temperatures used during HTC and, consequently, higher weight loss during post-pyrolysis treatment.

Moreover, the O/C atomic ratio was related to the content of oxygen-containing functional groups. As O/C increases, the polar oxygen functional groups increase [35]. As can be observed in Table 1, the post-pyrolyzed magnetic carbonaceous materials present lower O/C values than the non-pyrolyzed magnetic carbon nanocomposites (MAC, MCC, MHC$_{OR}$, MBC$_{SFH}$). Post-pyrolysis treatment significantly decreases the H/C atomic ratio indicating high aromaticity of post-pyrolyzed materials [36]. The lower H/C value of post-pyrolyzed materials corresponds to MACP, whereas the highest index corresponds to MCCP and MHCP$_{OR}$. Initially, MHC$_{OR}$ was the highest H/C atomic ratio material because hydrochar HC$_{OR}$ was obtained at the lowest temperature (240 °C) than BC$_{SFH}$ (700 °C) and commercial AC or CC. It is established that biochars present more aromatic and fewer aliphatic structures than hydrochars [37].

Finally, the pH of eight magnetic carbon nanocomposites are alkaline, ranging from 8.50 to 10.08 for MAC and MHCP$_{OR,}$ respectively. Post-pyrolysis treatment increases the pH in all cases due to ash enrichment and decarboxylation reactions. The highest increment is observed in the treatment of MHC$_{OR}$, according to H/C and O/C variations during post-pyrolysis. After post-pyrolysis treatment, magnetic carbonaceous materials show a more reductive character related to lower H/C ratios, with Eh values ranging from 250 to 287 mV. Finally, the EC shows significant variations: MAC, the material with a high EC value, and MHCP$_{OR}$ with the lowest.

3.1.3 Porosity development of magnetic carbon nanocomposites

Table 2 shows the BET surface area, pore-volume, and pore diameter obtained by BET and BJH models. MCNCs show values of BET surface areas between 57.69 and 511.43 m^2 g^{-1} for MCC and MAC, respectively. The BET surface area of MCC, MHC$_{OR,}$ or MBC$_{SFH}$ increases with post-pyrolysis treatment. However, MAC's BET surface area and pore volume slightly decreased from 511.43 to 425 m^2 g^{-1} and 0.131 to 0.120 cm^3 g^{-1}, respectively. This difference can be attributed to the sintering or collapse of tiny pores of MAC inside the carbon structure [38]. Moreover, the pore diameter of MAC, MC, and MBC decreases when samples
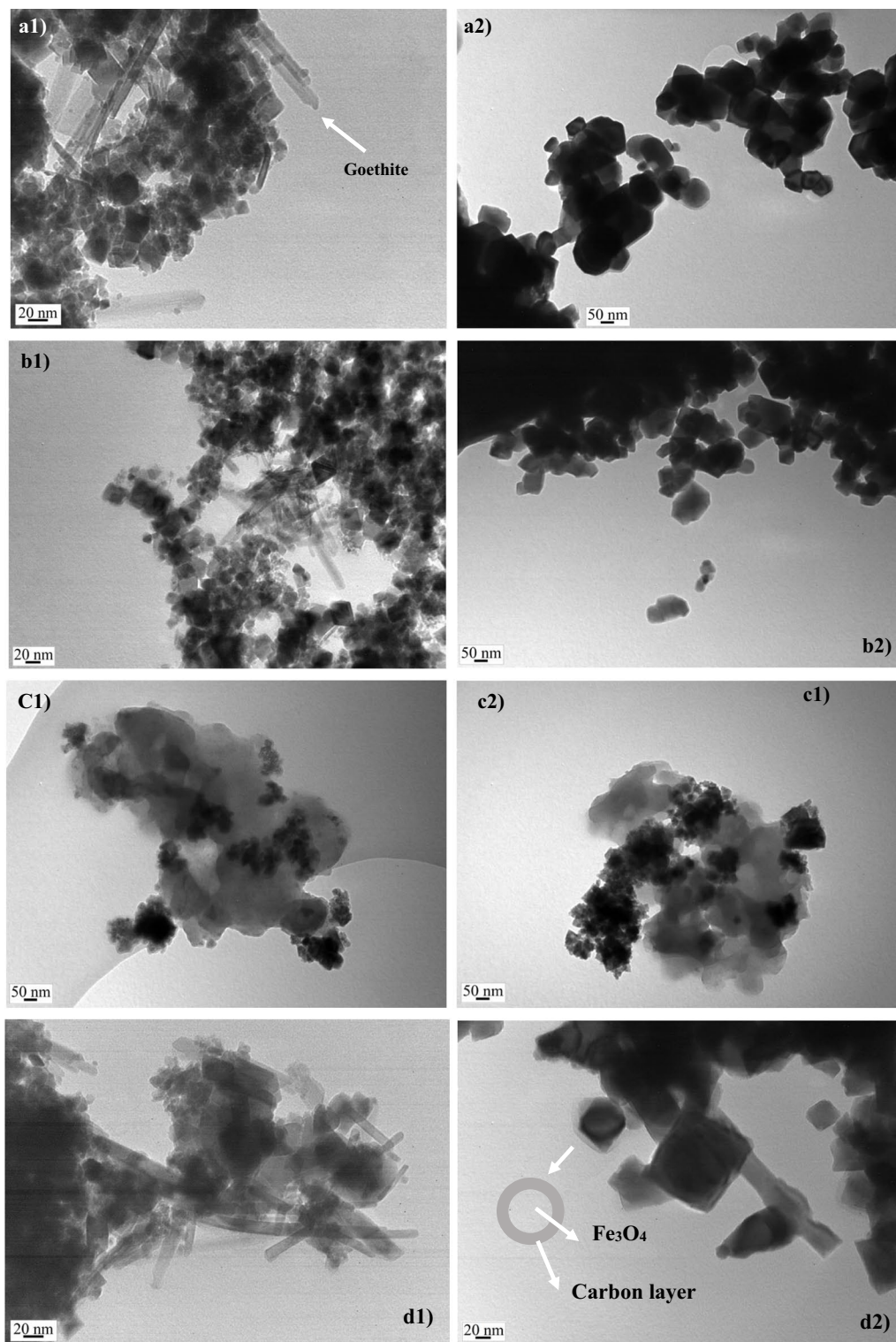
Fig. 2 TEM of (a1) MAC, (a2) MACP, (b1) MCC, (b2) MCCP, (c1) MHC$_{OR}$, (c2) MHCP$_{OR}$, (d1) MBC$_{SFH}$, and (d2) MBCP$_{SFH}$\

are post-pyrolyzed and increases in the case of MHC$_{OR}$ from 5.56 to 7.88 nm.

The N$_2$ adsorption–desorption isotherms are displayed in Fig. 3. As can be seen in the graphs, there is an important difference between isotherms of eight magnetic carbonaceous. MAC, MACP, MHC$_{OR}$, MHCP$_{OR}$, and MBC$_{SFH}$ maintained type IV isotherms related to mesoporous development. MCC and MCCP behave as type V, which is also

Table 1 Elemental analysis, pH, Eh, and electrical conductivity of magnetic carbon nanocomposites

Sample	C (%)	H (%)	N (%)	S (%)	O* (%)	O/C	H/C	Ash (%)	pH	Eh (mV)	$\sigma(\mu S/cm)$
MAC	47.25	0.46	0.00	0.09	2.37	0.04	0.11	49.83	8.50	320	772
MCC	35.74	1.56	0.00	0.00	9.15	0.19	0.52	53.54	9.50	331	151
MHC_{OR}	25.89	2.28	0.31	0.16	15.01	0.43	1.05	56.34	9.30	360	129
MBC_{SFH}	40.45	0.58	0.04	0.09	8.20	0.15	0.11	50.62	8.52	415	128
MACP	37.82	0.05	0.00	0.04	9.28	0.18	0.01	52.81	8.90	287	172
MCCP	33.70	0.34	0.00	0.00	6.86	0.15	0.12	59.09	9.73	257	268
$MHCP_{OR}$	20.22	0.21	0.16	0.12	6.05	0.22	0.12	73.23	10.08	250	74
$MBCP_{SFH}$	40.31	0.27	0.03	0.12	6.75	0.12	0.08	52.51	8.60	266	135

*Calculated by difference

Table 2 BET surface area, pore volume, and pore diameter of magnetic carbon nanocomposites

Material	S_{BET} (m^2 g^{-1})	Pore volume (cm^3 g^{-1})	Pore diameter (nm)
MAC	511.43 ± 1.27	0.131	6.44
MCC	57.69 ± 0.04	0.001	11.27
MHC_{OR}	83.47 ± 0.12	-	5.56
MBC_{SFH}	244.14 ± 0.58	0.075	7.87
MACP	425.00 ± 1.03	0.121	4.98
MCCP	120.41 ± 2.03	0.006	4.28
$MHCP_{OR}$	84.28 ± 0.95	0.021	7.88
$MBCP_{SFH}$	257.18 ± 0.96	0.076	4.61

associated with macroporous or non-porous materials [39, 40]. Besides, post-pyrolyzed magnetic carbon nanocomposites (MACP, MCCP, $MHCP_{OR}$, and $MBCP_{SFH}$) reached quantity adsorbed values lower than the initial carbon nanocomposites (MAC, MCC, MHC_{OR}, and MBC_{SFH}) suggesting that these materials possess different porous structures and pore sizes (the size of the hysteresis loop could qualitatively be taken as evidence of this) [41, 42]. MAC, MCC, MHC_{OR}, $MHCP_{OR}$, and MBC_{SFH} have an H3-type hysteresis loop associated with non-rigid aggregates of plate-like particles [43]. MACP and $MBCP_{SFH}$ are more likely to have H4, which might indicate the presence of a combination of micropores and mesopores [44].
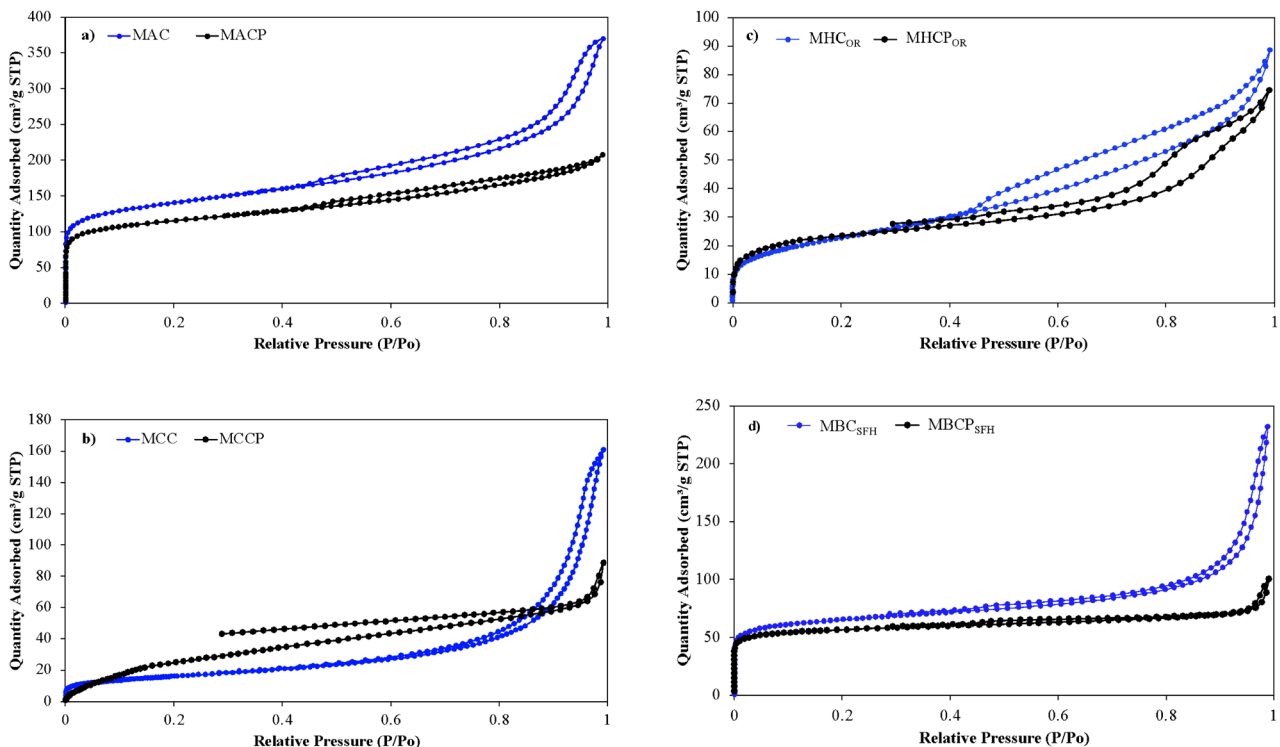
Fig. 3 N$_2$ adsorption–desorption isotherms of magnetic carbon nanocomposites

3.1.4 FTIR analysis

In Fig. 4, FTIR spectra of magnetic carbon nanocomposites are summarized. All spectra exhibit a stretching vibration mode around 500 cm^{-1} attributable to the Fe–O bond in iron oxide nanoparticles [45, 46]. This peak has subtly shifted and is more distorted in MACP, MCP, MHCP$_{OR}$, and MBCP$_{SFH}$, which might point to a partial coating of the magnetic core. Besides, the broad peak in the range $3300 - 3500$ cm^{-1} confirms the presence of the $O - H$ stretching vibration. This broad peak decreases its intensity in MACP and MHCPor spectra. Moreover, vibration bands at approximately 1600 cm^{-1}, corresponding to the stretching of $C = C$ groups, were observed in all samples, reflecting the aromatic rings present in the structure of each material.

3.1.5 Zeta potential

Zeta potential measurements as a function of pH are exhibited in Fig. 5. The graphs showed that the post-pyrolyzed magnetic carbon nanocomposites (MACP and MHCP$_{OR}$) reached a more negative zeta potential than the non-post-pyrolyzed materials in the pH range from 3 to 9. All magnetic carbon nanocomposites (MAC, MCC,

MHC$_{OR}$, MBC$_{SFH}$) possess an isoelectric point at different pH values. Nevertheless, when the materials suffered a post-pyrolysis treatment, the isoelectric point of MACP and MHCP$_{OR}$ is not visible, at least in the studied pH range. MCCP and MBCP$_{SFH}$ have an isoelectric point; at low pH values of approximately 3.8 and 3.5, respectively. The post-pyrolyzed magnetic carbon nanocomposites can acquire more negative zeta potential due to the partial coating of magnetite. These results suggest a more stable dispersion due to a possibly electrostatic stabilization in the colloidal system. The oxygen atoms in the carbonaceous matrixes are the ones that promote the repulsive forces.

3.1.6 Crystalline structure

Figure 6 shows the diffractograms of eight magnetic carbon nanocomposites. All samples show similar patterns related to the crystalline planes that could be indexed to the spinel inverse structure of magnetite (JCPDS 19–0629). It is essential to mention that it is not simple to differentiate crystalline planes of magnetite and maghemite since they possess the same cubic structure. Magnetite can be easily oxidized to maghemite. In this study, the synthesis procedure of magnetite was followed; it is
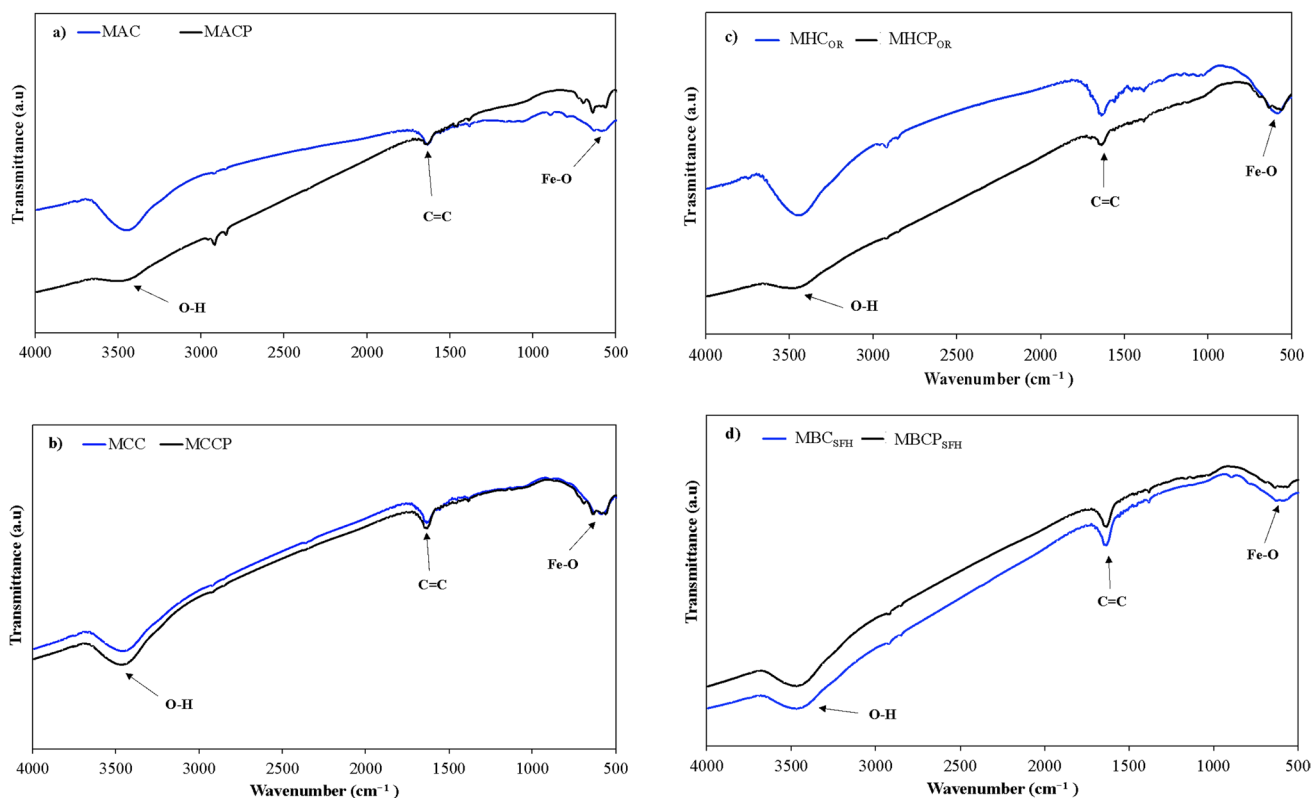

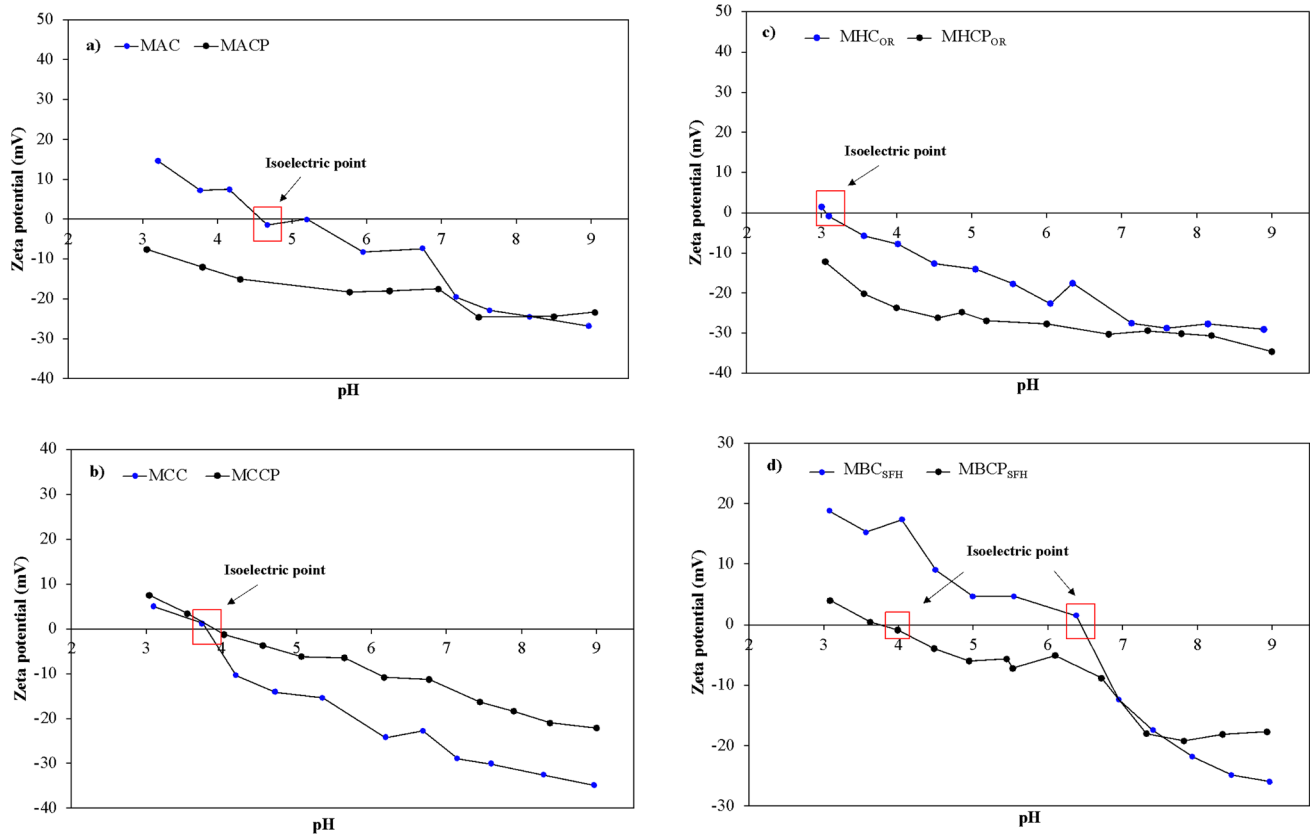**Fig. 4** FTIR of magnetic carbon nanocomposites

Fig. 5 Zeta potential as a function of pH of magnetic carbon nanocomposites

still challenging to ensure that the obtained iron oxide is magnetite. For this reason, it is suggested that there must be a mixture of magnetite/maghemite, expecting to have more magnetite. The prominent peaks obtained at around 23.87, 30.15, 35.52, 43.25, 53.60, 57.10, and 62.72° can be ascribed to (111), (200), (311), (440), (422), (511), and (499) planes, representative of Fe_3O_4. Additionally, some goethite crystalline planes are visible, standing out the one appearing at around 21° that is indexed to (110), which supports the idea of goethite transformation into other possible iron oxide phases such as hematite. This plane disappeared in the post-pyrolyzed magnetic carbonaceous diffractograms. In addition, when MAC, MCC, MHC_{OR}, and MBC_{SFH} are pyrolyzed, diffraction peaks seem sharpened. Furthermore, the wideband that appears between 20 and 30 is characteristic of the amorphous phase of carbonaceous materials [47].

3.2 Stability tests of magnetic carbonaceous materials

Figure 7 displays the concentration of Fe in a sulfuric acid solution to measure the stability of magnetic carbon

nanocomposites and post-pyrolyzed magnetic carbon nanocomposites. Each graph compares the magnetic carbonaceous material with the analogous post-pyrolyzed magnetic carbonaceous materials. At a strongly acidic medium (pH < 1), iron oxide nanoparticles are vulnerable to corrosion and post-dissolution by three main mechanisms reported in the literature: protonation, complexation, and reduction [48]. For this main reason, it is convenient to coat Fe_3O_4 nanoparticles to prevent this undesired effect of damaging and affecting the magnetic core. As can be seen in Fig. 7a, the carbon-coated materials that employed commercial activated carbon (MACP) and charcoal (MCCP) as the carbonaceous coatings suggest a non-homogenous coating of the magnetic core due to the high concentration of Fe (mg L^{-1}) in the solution, which indicated that Fe_3O_4 disaggregation occurred with H_2SO_4 solutions at 90 °C within 48 h of contact time. MAC and MACP leached more Fe than MCCP and MCC. Besides, MAC and MCC leached more Fe than MACP and MCCP, leading to Fe concentrations of 3430 and 802 mg L^{-1}, respectively.

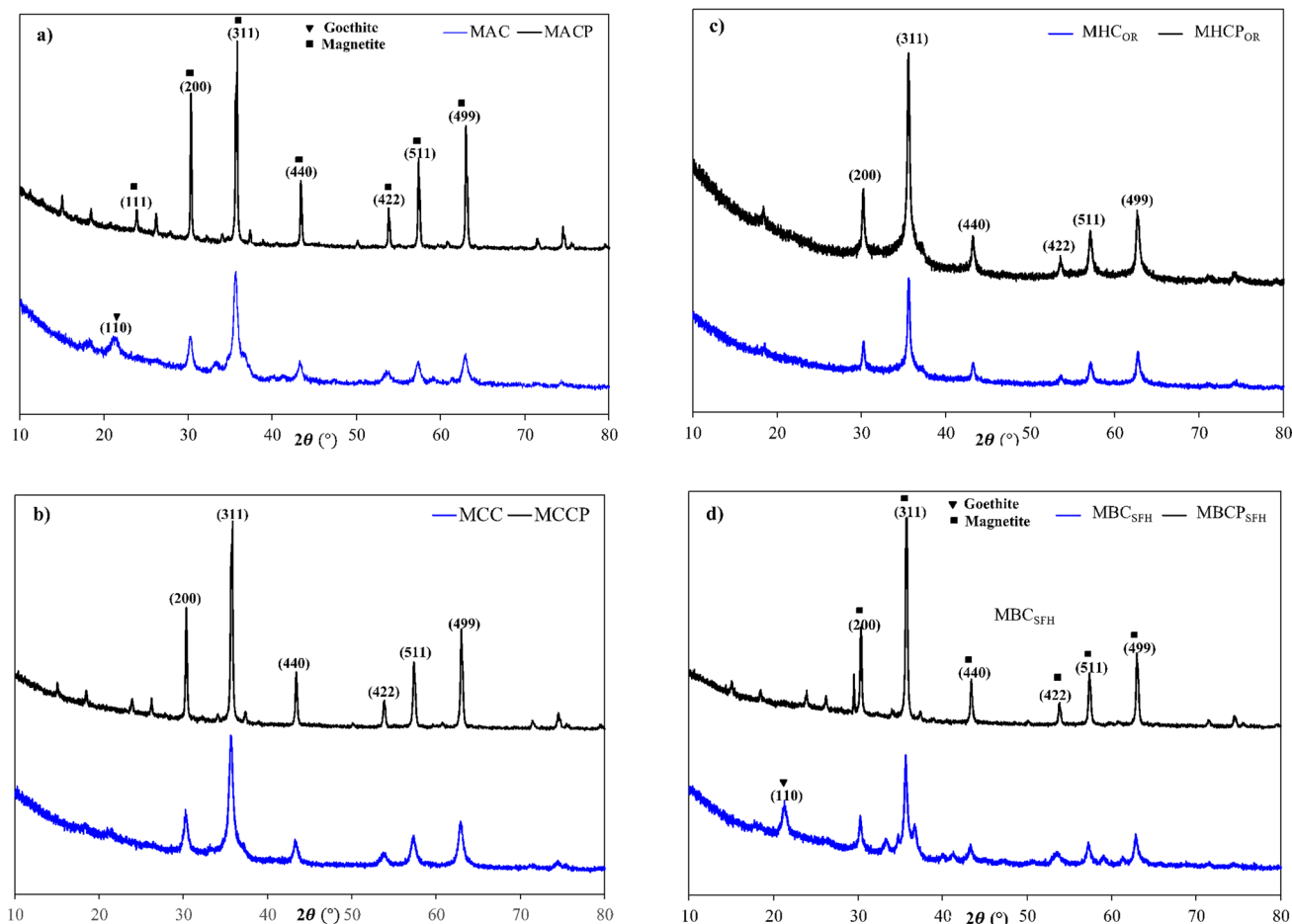On the other hand, when carrying out the stability test using the biochar and the hydrochar-based

Fig. 6 XRD of magnetic carbon nanocomposites

magnetic carbon nanocomposites (MHCP$_{OR}$, MHC$_{OR}$, MBCP$_{SFH}$, and MBC$_{SFH}$), Fe concentrations in the solution decreased considerably (Fig. 7b). From both materials, coated originated during post-pyrolysis treatment of MBCP$_{SFH}$ acts as a better stabilizer and more effective coating, reducing Fe leaching into the acidic medium, achieving values up to 163 mg L^{-1} within 48 h of leaching at 90 °C. Moreover, when employing MHC$_{OR}$ and MBC$_{SFH}$ (the non-coated magnetic carbon–based materials), Fe concentration increased in the medium, pointing out a partial encapsulation that protects magnetite nanoparticles when coating the magnetic core. It is suggested that temperature (when pyrolyzed the magnetic carbon nanocomposites) promotes the releasing of volatiles from biochar and hydrochar carbon matrix which, by physical or chemical interactions, lead to formation of carbon structures deposited on the magnetite surface.

3.2.1 Magnetic properties

The biochar and the hydrochar-based magnetic carbon nanocomposites (MHCP$_{OR}$, MHC$_{OR}$, MBCP$_{SFH}$, and MBC$_{SFH}$) were selected for subsequent analysis of magnetic properties. The four magnetic carbon nanocomposites exhibit superparamagnetic properties characteristic of single-domain ferro- or ferrimagnetic particles with sizes below approximately 50 nm. The coercive fields vary between 6 and 18 mT, the MBCP$_{SFH}$ being greater. This sample presents the largest dipole moment of np and the largest estimated size of the magnetic core. The least coercive corresponds to MBC$_{SFH}$. Saturation magnetizations are below 1.4 Am^2 kg^{-1} (MHCP$_{or}$) and above 0.3 Am^2 kg^{-1} (MHC$_{OR}$). These are very small values compared to those of the magnetite and maghemite phases, which implies that these phases are minor components of the samples; hence,

Fig. 7 Stability test in terms of iron leaching of magnetic carbon nanocomposites
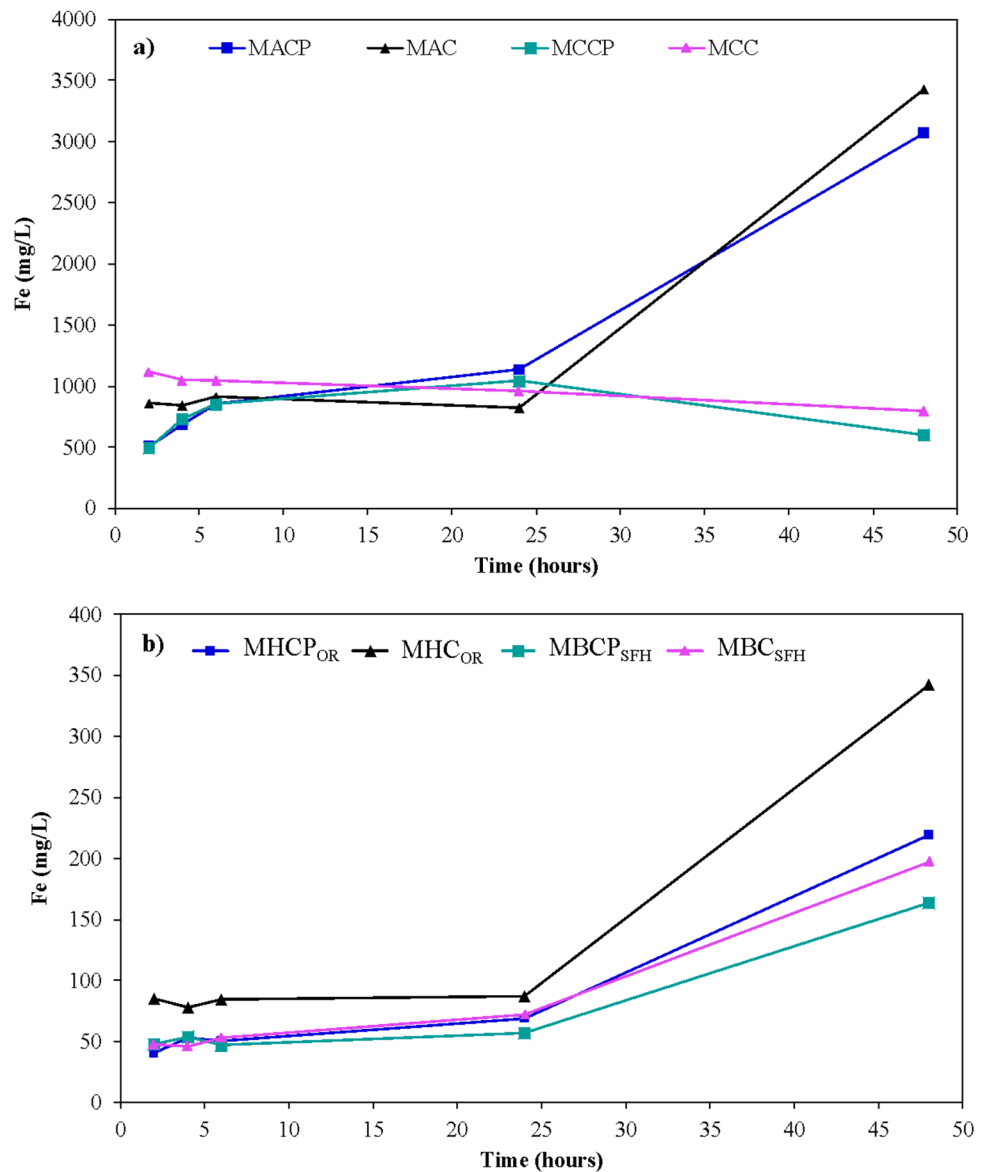
the coating mass reduces the specific moment Ms of the samples. The potential fractions of these phases were estimated from the magnetizations obtained and those reported in the literature for the pure phases at RT (93 Am^2 kg^{-1} for magnetite and 76 Am^2 kg^{-1} for maghemite). As observed in Fig. 8a, MBC$_{SFH}$ shows a higher M$_s$ than MBC$_{SFH}$ [49–51].

On the contrary, Fig. 8b, suggests that MHCP$_{OR}$ reaches greater M$_s$. Both materials have suffered the same thermal treatment at 600 °C. Their difference lies in the amorphous carbon matrix employed (biochar and hydrochar, respectively). Possible interpretations are that the nanoparticles are stone/layer with thick carbon layers or that the sample is a mixture of NP stone/layer and other structures of a carbon-based majority non-magnetic phase.

The dipole moments (in Table 3) of np obtained depend on the fitting method. Langevin-type settings vary between 13,300 (MHCP$_{OR}$) and 20,300 μ_B (MBCP$_{SFH}$), for Chantrell's definitions, between 6100 (MHCP$_{SFH}$) and 19,100 μ_B ((MBCP$_{SFH}$). There is consistency in relative values but an appreciable difference in absolute values. Their relative standard deviations are generally close to 1 (the largest are those of MBC$_{SFH}$ and MHCP$_{SFH}$, > 1 for both adjustment models). The relative standard deviation of MBCP$_{SFH}$ is the smallest of all, and the magnetic pits of this sample are less scattered. The low value obtained from the Langevin analysis (< 0.02) is striking. This result suggests that, since NPs are not in a colloidal medium but are part of a powder with limited motion freedom, the Chantrell approach is the most appropriate for analyzing the magnetization cycles.

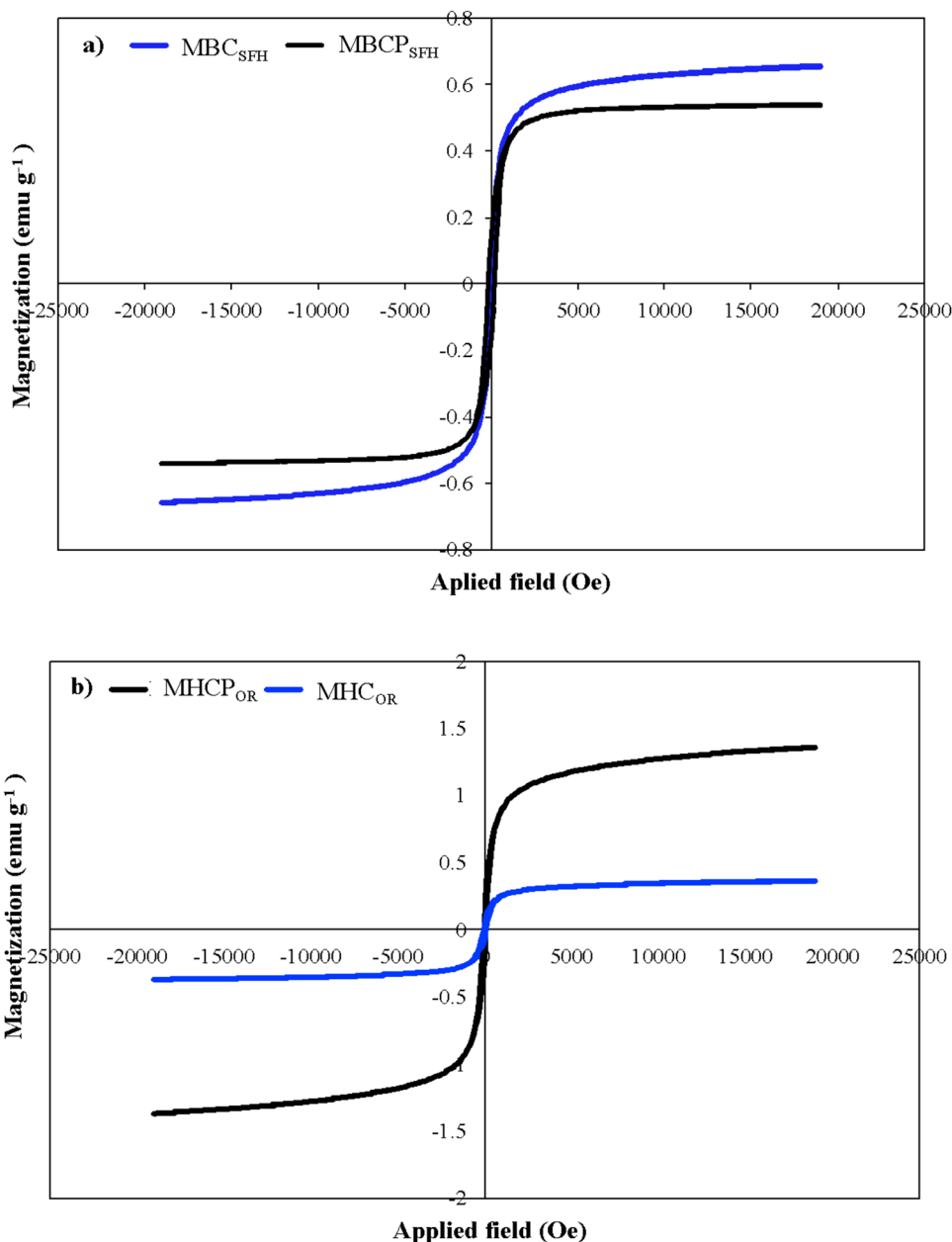**Fig. 8** Magnetic properties of magnetic carbon nanocomposites

Table 3 Magnetic parameters of magnetic carbon nanocomposites MBC_{sfh}, $MBCP_{sfh}$, MHC_{or} and $MHCP_{or}$

Sample	Hc (mT)	D_Ch (nm)	D_Lan (nm)	Ms Lan (Am² kg⁻¹)	Ms Ch (Am² kg⁻¹)	Ch<u>(u_B)	Lan<u>(u_B)
MBC_{SFH}	5.86	7.20	8.80	0.62	0.65	7929	14476
$MBCP_{SFH}$	17.45	9.80	9.90	0.55	0.54	19650	20318
MHC_{OR}	10.26	7.00	9.20	0.34	0.36	7192	16372
$MHCP_{OR}$	7.64	6.60	8.60	12.16	132.452	6059	13295

The mean volumes of the magnetic pits are calculated by dividing the mean moment of np by the saturation magnetization of the magnetic phase, which was arbitrarily assumed to be 75 emu/g.

$$< V > = < \mu > /M_S$$

The estimated values of the diameters (assuming spherical pits)

$$< D >= (6 < V > /\pi)^{1/3}$$

are between 6.6 and 9.9 nm; the largest, 9.8–9.9 nm, corresponds to MBCP, and the smallest, 6.6–8.6 nm (depending on the fit model), to MHCP$_{OR}$. The most uniform resulting sizes using Langevin analysis, in this case, is in the range of 8.6–9.9 nm for all samples [52–54].

4 Conclusions

Magnetic carbon nanocomposites were prepared using a co-precipitation method followed by post-pyrolysis treatment at 600 °C. The main conclusions are the following:

Post-pyrolysis treatment of magnetic carbon nanocomposites converts goethite (a reaction intermediate) into a possible hematite phase. Core–shell systems are possibly formed with a thin carbon coating encapsulating the iron oxide nanoparticles.

The post-pyrolyzed magnetic carbon nanocomposites gained more negative zeta potential.

Post-pyrolysis treatment increases the aromaticity of carbon structures. In contrast, the BET surface area shows low deviations for hydrochar, biochar, and charcoal-based materials and slight decreases for magnetic carbon nanocomposites prepared using activated carbon.

Post-pyrolysis treatment increases the stability of magnetic carbon nanocomposites in an acidic medium, decreasing the leaching of iron indicating that the coat generated during post-pyrolysis could partially protect the magnetic core by reducing Fe leaching into the acidic aqueous medium. Magnetic carbon nanocomposites obtained from biochar and hydrochar show lower iron leaching than those from commercial charcoal or activated carbon indicating the highest stability of carbon coating.

The biochar and the hydrochar-based magnetic carbon nanocomposites before and after post-pyrolysis treatment exhibit superparamagnetic properties. The saturation magnetization decreased as the coating layer became denser because of a dead layer around the magnetic core. The reduction in the core size also contributed to the lowered in the M$_s$ values.

These results open the potential application fields of magnetic carbon nanocomposites obtained by in situ co-precipitation of magnetite nanoparticles into biochar and hydrochar-based-carbonaceous materials and post-pyrolysis treatment in acidic mediums.

Data availability Not applicable.

Declarations

Ethical approval Not applicable.

Conflict of interest The authors declare no competing interests.

References

1. Jacinto MJ, Silva VC, Valladão DMS, Souto RS (2021) Biosynthesis of magnetic iron oxide nanoparticles: a review. Biotechnol Lett 43:1–12. https://doi.org/10.1007/s10529-020-03047-0

2. Marcelo LR, de Gois JS, da Silva AA, César DV (2021) Synthesis of iron-based magnetic nanocomposites and applications in adsorption processes for water treatment: a review. Environ Chem Lett 19:1229–1274. https://doi.org/10.1007/s10311-020-01134-2

3. Shete PB, Patil RM, Tiwale BM, Pawar SH (2015) Water dispersible oleic acid-coated Fe$_3$O$_4$ nanoparticles for biomedical applications. J Magn Magn Mater 377:406–410. https://doi.org/10.1016/j.jmmm.2014.10.137

4. Sengul AB, Asmatulu E (2020) Toxicity of metal and metal oxide nanoparticles: a review. Environ Chem Lett 18:1659–1683. https://doi.org/10.1007/s10311-020-01033-6

5. Razavi R, Amiri M, Salavati-Niasari M (2022) Eco-friendly synthesis by Rosemary extract and characterization of Fe$_3$O$_4$@

SiO$_2$ magnetic nanocomposite as a potential adsorbent for enhanced arsenic removal from aqueous solution: isotherm and kinetic studies. Biomass Conv Bioref. https://doi.org/10.1007/s13399-022-02489-y

6. ShiraghaeiKoutenaei S, Vatankhah G, Esmaeili H (2022) Ziziphus spina-christi leaves biochar decorated with Fe$_3$O$_4$ and SDS for sorption of chromium (III) from aqueous solution. Biomass Conv Bioref. https://doi.org/10.1007/s13399-022-03029-4

7. Shahrashoub M, Bakhtiari S (2021) The efficiency of activated carbon/magnetite nanoparticles composites in copper removal: Industrial waste recovery, green synthesis, characterization, and adsorption-desorption studies. Microporous Mesoporous Mater 311:110692. https://doi.org/10.1016/j.micromeso.2020.110692

8. Xu J, Liu Z, Zhao D, Gao N, Fu X (2020) Enhanced adsorption of perfluorooctanoic acid (PFOA) from water by granular activated carbon supported magnetite nanoparticles. Sci Total Environ 723:137757. https://doi.org/10.1016/j.scitotenv.2020.137757

9. Yihunu EW, Minale M, Abebe S, Limin M (2019) Preparation, characterization and cost analysis of activated biochar and hydrochar derived from agricultural waste: a comparative study. SN Appl Sci 1:873. https://doi.org/10.1007/s42452-019-0936-z

10. Sri Shalini S, Palanivelu K, Ramachandran A, Raghavan V (2021) Biochar from biomass waste as a renewable carbon material for climate change mitigation in reducing greenhouse gas emissions-a review. Biomass Conv Bioref 11:2247–2267. https://doi.org/10.1007/s13399-020-00604-5

11. Scheverin VN, Horst MF, Lassalle VL (2022) Novel hydroxyapatite-biomass nanocomposites for fluoride adsorption. Results Eng 16:100648. https://doi.org/10.1016/j.rineng.2022.100648

12. Gong H, Chi J, Ding Z, Zhang F, and Huang J (2020) Removal of lead from two polluted soils by magnetic wheat straw biochars. Ecotoxicol Environ Safety 205:111132. https://doi.org/10.1016/j.ecoenv.2020.111132

13. Álvarez ML, Gascó G, Rodríguez-Pacheco R, Paz-Ferreiro J, Méndez A (2022) Recovery of metals from mine wastes: The effect of biochar–Fe composites in the immobilization of arsenic. J Sustain Metall 8:419–229. https://doi.org/10.1007/s40831-022-00495-y

14. Méndez A, Álvarez ML, Fidalgo JM, Di Stasi C, Manyà JJ, Gascó G (2022) Biomass-derived activated carbon as catalyst in the leaching of metals from a copper sulfide concentrate. Miner Eng 186:107594. https://doi.org/10.1016/j.mineng.2022.107594

15. Wang JN, Zhang L, Yu F, Sheng ZM (2007) Synthesis of carbon encapsulated magnetic nanoparticles with giant coercivity by a spray pyrolysis approach. J Phys Chem B 111:2119–2124. https://doi.org/10.1021/jp0674118

16. Lyubutin IS, Lin CR, Tseng YT, Spivakov A, Baskakov AO, Starchikov SS, Funtov JO, Jhang CJ, Tsai YJ, Hsu HS (2019) Structural and magnetic evolution of FexOy @carbon core-shell nanoparticles synthesized by a one-step thermal pyrolysis. Mater Charact 150:213–219. https://doi.org/10.1016/j.matchar.2019.02.022

17. Sun YH, Liu S, Zhou FC, Nan JM (2016) Electrochemical performance and structure evolution of core-shell nano-ring α-Fe$_2$O$_3$@Carbon anodes for lithium-ion batteries. Appl Surf Sci 390:175–184. https://doi.org/10.1016/j.apsusc.2016.08.071

18. Ma C, Luo B, Song HH, Zhi LJ (2010) Preparation of carbon-encapsulated metal magnetic nanoparticles by an instant pyrolysis method. New Carbon Mater 25:199–204. https://doi.org/10.1016/S1872-5805(09)60028-7

19. Da Costa TR, Baldi E, Figueiró A, Colpani GK, Silva LL, Zanetti M, De Mello JMM, Fiori M A (2019) Fe$_3$O$_4$@C core-shell nanoparticles as adsorbent of ionic zinc: Evaluating of the adsorptive capacity. Mater Res 22. https://doi.org/10.1590/1980-5373-MR-2018-0847

20. Kang J, Kim Y, Kim HM, Hu X, Saito N, Choi JH, Lee MH (2016) In-situ one-step synthesis of carbon-encapsulated naked magnetic metal nanoparticles conducted without additional reductants and agents. Sci Rep 6:38652. https://doi.org/10.1038/srep38652

21. Lee JS, Song YJ, Hsu HS, Lin CR, Huang JY, Chen J (2019) Magnetic enhancement of carbon-encapsulated magnetite nanoparticles. J Alloys Compd 790:716–722. https://doi.org/10.1016/j.jallcom.2019.03.191

22. Yu F, Wang JN, Sheng ZM, Su LF (2005) Synthesis of carbon-encapsulated magnetic nanoparticles by spray pyrolysis of iron carbonyl and ethanol. Carbon 43:3018–3021. https://doi.org/10.1016/j.carbon.2005.06.008

23. Ahmadpoor F, Masood A, Feliu N, Parak WJ, Shojaosadati SA (2021) The effect of surface coating of iron oxide nanoparticles on magnetic resonance imaging relaxivity. Front Nanosci 3:644734. https://doi.org/10.3389/fnano.2021.644734

24. Mylkie K, Nowak P, Rybczynski P, Ziegler-Borowska M (2021) Polymer-coated magnetite nanoparticles for protein immobilization. Materials 14:248. https://doi.org/10.3390/ma14020248

25. Barry D, Barbiero C, Briens C, Berruti F (2019) Pyrolysis as an economical and ecological treatment option for municipal sewage sludge. Biomass Bioenerg 122:472–480. https://doi.org/10.1016/j.biombioe.2019.01.04

26. Martínez-Prieto LM, Marbaix J, Asensio JM, Cerezo-Navarrete C, Fazzini PF, Soulantica K, Chaudret B, Corma A (2020) Ultrastable magnetic nanoparticles encapsulated in carbon for magnetically induced catalysis. ACS Appl Nano Mater 3:7076–7087. https://doi.org/10.1021/acsanm.0c01392

27. Yeap SP, Lim KK, Ooi BS, Ahmad AL (2017) Agglomeration, colloidal stability, and magnetic separation of magnetic nanoparticles: collective influences on environmental engineering applications. J Nanoparticle Res 19:368. https://doi.org/10.1007/s11051-017-4065-6

28. Tang SCN, Lo IMC (2013) Magnetic nanoparticles: Essential factors for sustainable environmental applications. Water Res 47:2613–2632. https://doi.org/10.1016/j.watres.2013.02.039

29. Golas PL, Louie S, Lowry GV, Matyjaszewski K, Tilton RD (2010) Comparative study of polymeric stabilizers for magnetite nanoparticles using ATRP. Langmuir 26:16890–16900. https://doi.org/10.1021/la103098q

30. He YT, Traina SJ (2007) Transformation of magnetite to goethite under alkaline pH conditions. Clay Miner 42:13–19. https://doi.org/10.1180/claymin.2007.042.1.02

31. Gualtieri AF, Venturelli P (1999) In situ study of the goethite-hematite phase transformation by real time synchrotron powder diffraction. Am Min 84:884–894. https://doi.org/10.2138/am-1999-5-624

32. Walter D, Buxbaum G, Laqua W (2001) The mechanism of the thermal transformation from goethite to hematite. J Therm Anal Calorim 63:733–748. https://doi.org/10.1023/A:1010187921227

33. Gialanella S, Girardi F, Ischia G, Lonardelli I, Mattarelli M, Montagna M (2010) On the goethite to hematite phase transformation. J Therm Anal Calorim 102:867–873. https://doi.org/10.1007/s10973-010-0756-2

34. Deng J, Ren P, Deng D, Bao X (2015) Enhanced electron penetration through an ultrathin graphene layer for highly efficient catalysis of the hydrogen evolution reaction. Angewandte Chemie-International Edition 54:2100–2014. https://doi.org/10.1002/anie.201409524

35. Rafiq MK, Bachmann RT, Rafiq MT, Shang Z, Joseph S, Long RL (2016) Influence of pyrolysis temperature on physico-chemical properties of corn stover (zea mays l.) biochar and feasibility for carbon capture and energy balance. PLoS One 11:e0156894. https://doi.org/10.1371/journal.pone.0156894

36. Cao Q, An A, Xie J, Liu Y, Xing L, Ling X, Chen C (2022) Insight to the physiochemical properties and DOM of biochar under different pyrolysis temperature and modification conditions. J Anal Appl Pyrolysis 166:105590. https://doi.org/10.1016/j.jaap.2022.105590

37. Gascó G, Paz-Ferreiro J, Álvarez ML, Saa A, Méndez A (2018) Biochars and hydrochars prepared by pyrolysis and hydrothermal carbonisation of pig manure. Waste Managem 79:395–403. https://doi.org/10.1016/j.wasman.2018.08.015

38. Nandi M, Okada K, Dutta A, Bhaumik A, Maruyama J, Derks D, Uyama H (2012) Unprecedented CO_2 uptake over highly porous N-doped activated carbon monoliths prepared by physical activation. ChemComm 48:10283–10285. https://doi.org/10.1039/c2cc35334b

39. Alothman ZA (2012) A review: Fundamental aspects of silicate mesoporous materials. Materials 5:2874–2902. https://doi.org/10.3390/ma5122874

40. Broekhoff JCP (1979) Mesopore determination from nitrogen sorption isotherms: Fundamentals, scope, limitations. Stud Surf Sci Catal 3:663–684. https://doi.org/10.1016/S0167-2991(09)60243-3

41. Liu F, Dai Y, Zhang S, Li J, Zhao C, Wang Y, Liu C, Sun J (2018) Modification and application of mesoporous carbon adsorbent for removal of endocrine disruptor bisphenol A in aqueous solutions. J Mater Sci 53:2337–2350. https://doi.org/10.1007/s10853-017-1705-2

42. Zhang J, Jiang P, Shen Y, Zhang W, Bian G (2016) Covalent anchoring of Mo(VI) Schiff base complex into SBA-15 as a novel heterogeneous catalyst for enhanced alkene epoxidation. J Porous Mater 23:431–440. https://doi.org/10.1007/s10934-015-0097-4

43. Fuertes AB, Arbestain MC, Sevilla M, Maciá-Agulló JA, Fiol S, López R, Smernik RJ, Aitkenhead WP, Arce F, Macias F (2010) Chemical and structural properties of carbonaceous products obtained by pyrolysis and hydrothermal carbonisation of corn stover. Aust J Soil Res 48:618–626. https://doi.org/10.1071/SR10010

44. Anfar Z, Ait Ahsaine H, Zbair M, Amedlous A, Ait El Fakir A, Jada A, El Alem N (2020) Recent trends on numerical investigations of response surface methodology for pollutants adsorption onto activated carbon materials: A review. Crit Rev Environ Sci Technol 50:1043–1084. https://doi.org/10.1080/10643389.2019.1642835

45. Singh A, Sahoo SK (2014) Magnetic nanoparticles: A novel platform for cancer theranostics. Drug Discovery Today 19:474–481. https://doi.org/10.1016/j.drudis.2013.10.005

46. He YP, Wang SQ, Li CR, Miao YM, Wu ZY, Zou BS (2005) Synthesis and characterization of functionalized silica-coated Fe_3O_4 superparamagnetic nanocrystals for biological applications. J Phys D Appl Phys 38:1342–1350. https://doi.org/10.1088/0022-3727/38/9/003

47. Manoj B, Kunjomana AG (2012) Study of Stacking Structure of Amorphous Carbon by X-Ray Diffraction Technique Int. J Electrochem Sci 7:3127–3134

48. Wang D, Guan K, Bai Z, Liu F (2016) Facile preparation of acid-resistant magnetite particles for removal of Sb(III) from strong acidic solution. Sci Technol Adv Mater 17:80–88. https://doi.org/10.1080/14686996.2016.1145530

49. Cheng S, Pan X, Zhang C, Lin X, Zhuang Q, Jiao Y, Dong W, Qi X (2022) UV-assisted ultrafast construction of robust Fe_3O_4/polydopamine/Ag Fenton-like catalysts for highly efficient micropollutant decomposition. Sci Total Environ 810:151182. https://doi.org/10.1016/j.scitotenv.2021.151182

50. Cheng S, Zhang C, Li J, Pan X, Zhai X, Jiao Y, Li Y, Dong W, Qi X (2021) Highly efficient removal of antibiotic from biomedical wastewater using Fenton-like catalyst magnetic pullulan hydrogels. Carbohydr Polym 262:117951. https://doi.org/10.1016/j.carbpol.2021.117951

51. Pan X, Cheng S, Zhang C, Jiao Y, Lin X, Dong W, Qi X (2021) Mussel-inspired magnetic pullulan hydrogels for enhancing catalytic degradation of antibiotics from biomedical wastewater. Chem Eng J 409:128203. https://doi.org/10.1016/j.cej.2020.128203

52. Tiwari A, Verma NC, Turkkan S, Debnath A, Singh A, Draeger G, Nandi CK, Randhawa JK (2020) Graphitic carbon coated magnetite nanoparticles for dual mode imaging and hyperthermia. ACS Appl Nano Mater 3:896–904. https://doi.org/10.1021/acsanm.9b02501

53. Malhotra N, Audira G, Chen JR, Siregar P, Hsu HS, Lee JS, Ger TR, Hsiao CD (2020) Surface modification of magnetic nanoparticles by carbon-coating can increase its biosafety: evidences from biochemical and neurobehavioral tests in Zebrafish. Molecules 9:2256. https://doi.org/10.3390/molecules25092256

54. Arana M, Jacobo SE, Troiani H, Bercoff PG (2013) Synthesis and characterization of carbon-coated magnetite for functionalized ferrofluids. IEEE Trans Magn 8:4547–4550. https://doi.org/10.1109/TMAG.2013.2259805